INFINITESIMAL PHASE RESPONSE CURVES FOR PIECEWISE

SMOOTH DYNAMICAL SYSTEMS

by

Youngmin Park

Submitted in partial fulfillment of the requirements

For the degree of Masters of Science

Thesis Advisor: Dr. Peter J. Thomas

Department of Mathematics

CASE WESTERN RESERVE UNIVERSITY

August, 2013

CASE WESTERN RESERVE UNIVERSITY

SCHOOL OF GRADUATE STUDIES

We hereby approve the thesis/dissertation of

Youngmin Park

candidate for the _____ Masters of Science _____ degree*.

Peter J. Thomas (committee chair)

Hillel J. Chiel

Alethea Barbaro

Michael G. Hurley

(date)_____ August, 2013 _____

*We also certify that written approval has been obtained for any

proprietary material contained therein.

Dedication

For my father, Pilho, and sister, Young-Eun.

Contents

References   **55**

List of Tables

List of Figures

List of Abbreviations

CPG Central Pattern Generator

DI Differential Inclusion

iPRC Infinitesimal Phase Response Curve

NW Northwest

PRC Phase Response Curve

PML Piecewise Linear Morris-Lecar

PWL Piecewise Linear

PWLDS Piecewise Linear Dynamical System

$\mathbb{R}$ The Real Numbers

$\mathbb{R}^+$ The nonnegative real numbers

SW Southwest

$||\cdot||$ Arbitrary Norm

Acknowledgements

Special thanks to Dr. Thomas, Dr. Chiel, and Kendrick Shaw for their unwa-

vering guidance and support.

Abstract

Dynamical systems with discontinuous right-hand sides are utilized to great effect in mathematical biology (Coombes 2008, Glass and Kauffman 1973, McKean 1970), including models of central pattern generators (CPGs) involved in motor control (Spardy et al. 2011, Shaw et al. 2012). CPG models typically exhibit limit cycle dynamics; the infinitesimal phase response curve (iPRC) quantifies sensitivity of such models to external inputs (Ermentrout and Terman 2010). Piecewise smooth dynamical systems may have discontinuous iPRCs. In this thesis, we formulate the boundary conditions necessary for obtaining the iPRC for general piecewise smooth dynamical systems by solving an adjoint equation, thereby improving upon two known methods used to solve for the iPRC in the context of piecewise linear dynamical systems.

1 Introduction

Central pattern generators (CPGs) are networks of neurons that produce rhythmic outputs even in the absence of sensory feedback. Some rhythmic processes controlled by CPGs include breathing (by the pre-Bötzinger complex in mammals [3, 4]), locomotion [5, 21, 22], and mastication [15]. CPGs may be modeled using limit cycles, with the CPG circuit embedded inside biomechanical systems. These systems are often subject to environmental variability, which may include loads and mechanical resistance. In many circumstances, it would be disadvantageous if the motion produced by the CPG did not take into account these external forces. For a simple example of how CPGs robustly adapt to forces, imagine chewing hard bubble gum. Stiff gum requires extra force to soften, leading to an increase in the duration of a chewing cycle [18]. In general, an animal may need to apply a force for longer or shorter times, which could be accomplished by lengthening or shortening the time spent in a portion of a CPG limit cycle.

In [20], Shaw et al. hypothesized that the relative timing of different components of feeding motions could be controlled by manipulating the proximity of trajectories to equilibrium points. We are interested in this possibility as a mechanism for controlling timing. Experimental observations suggest the underlying dynamics of the CPG could consist of a limit cycle passing closer to or farther from one or more fixed points. External or internal perturbations

that shift near-limit cycle trajectories closer or father from fixed points could thereby slow down or speed up these trajectories, providing a mechanism for significantly changing the duration of a particular phase of a CPG cycle.

Infinitesimal phase response curves (iPRCs) quantify changes in timing of an oscillator in response to perturbations. iPRCs arise from the reduction of an oscillator to a single phase variable, which we will discuss further below. In [20], Shaw et al. analyzed a one-parameter family of planar differential equations with limit cycles whose proximity to fixed points varied parametrically. They discovered anomalous structure in the shape of the iPRC and the sensitivity of the underlying limit cycle. In order to carry out a more complete analysis of the shape of the iPRC, Shaw et al. constructed a related family of piecewise linear (PWL) planar differential equations (the iris system, defined in Appendix A.2.5). The analytical tractability of this system led to the exact derivation of an iPRC, which provided insight into the behavior of the smooth nonlinear system.

Differential equations where the right hand side is piecewise continuous, on a collection of domains partitioning the phase space, is a generalization of smooth differential equations, and are referred to as differential inclusions (DIs) [9]. DIs, discussed further in Section 1.2, appear in a variety of contexts including control theory [17], as well as in mathematical biology for modeling rhythmic processes. For example, the switch between swing and stance in models of bipedal animals or quadrupeds is represented by defining two sets

of differential equations, and switching the dynamics by a threshold condition [21, 22]. In addition, piecewise linear DIs have proved useful as approximations to biological dynamics modeled by smooth systems. In the study of gene regulatory networks, piecewise linear dynamical systems (PWLDS) play an important role in modeling gene regulatory networks (Glass networks) [11]. In some networks, genes switch almost instantaneously and determine a new set of rules for protein production. This rapid switch is assumed to be instantaneous, and the protein production dynamics are assumed to be linear, leading to a system of piecewise linear (PWL) differential equations [10]. In the study of gap junction coupled neural networks, PWL approximations to smooth systems allow for analytical solutions which would not be available in the corresponding smooth system [6]. In order to study the limit cycles approaching a sequence of saddle equilibria, we will consider PWL systems where each domain contains a saddle point with the dynamics determined by the linearization about the corresponding saddle of the smooth system.

For limit cycles in general nonlinear systems of differential equations, an explicit expression for the iPRC is known in only a few cases [2]. In most cases, the iPRC must be obtained through an approximation, typically by numerical integration of an adjoint equation (Section 1.1 and Appendix A.1). Shaw et al. used a direct approach by combining the effects of perturbations on timing and position of trajectories, deriving an exact iPRC with discontinuous jumps at some boundaries and not at others [20]. Coombes studied two piecewise linear

models that have continuous iPRCs and formulated a derivation for the iPRC that applies naturally to both models (and indeed similar classes of FitzHugh-Nagumo-type models) [6]. However, the approach in [6] does not take into account possible discontinuities in the iPRC (such as those in the iris system, Appendix A.3 and A.2.5). In this thesis, we provide a concise, closed-form analytic expression for the discontinuity of the iPRC at the domain boundary of any planar piecewise linear differential equation, as well as for more general DIs including nonlinear piecewise smooth differential equations, satisfying a natural boundary condition. This expression, combined with a solution to the adjoint equation (solvable in closed form for piecewise linear domains), provides a complete picture of the iPRC for a broad class of planar piecewise smooth differential equations.

1.1 Phase Response Curves and the Adjoint Equation

The phase response curve (PRC) is a periodic function quantifying the change in timing of a limit cycle in response to instantaneous perturbations of a trajectory. Perturbations may include mechanical feedback, proprioceptive feedback, or input from neighboring oscillators. Here, we focus on mechanical and proprioceptive feedback. The techniques of linear perturbation theory dictate the use of small perturbations. Moreover, in the study of near-homoclinic or near-heteroclinic systems, basins of attraction are often small. In the limit of small

perturbations, one obtains the infinitesimal phase response curve (iPRC).

The iPRC is typically defined in the context of smooth systems [8]. Here, we explore the validity of the iPRC and related tools in the context of piecewise smooth and piecewise linear dynamical systems. For the convenience of the reader, we review the classical terms needed to define the iPRC and the adjoint equation that it satisfies. Then we examine how these notions extend to limit cycles arising from piecewise smooth dynamics.

Consider a deterministic system of autonomous ordinary differential equations in $\mathbb{R}^n$ with smooth right-hand side:

$$\frac{dx}{dt} = F(x), \tag{1}$$

where $F : \mathbb{R}^n \to \mathbb{R}^n$ is a C^∞ map.

Definition 1 *A non-constant solution $x(t)$ (with initial condition $x(0) = x_0$) is called* <u>*periodic*</u> *with period T if there exists a real constant T such that*

$$x(t) = x(t + T), \quad \forall t \in \mathbb{R}^+, \tag{2}$$

where $T > 0$ is the least such number.

Definition 2 *A T-periodic stable limit cycle, γ, is an isolated T-periodic solution with the property that nearby solutions converge to the set $\Gamma = \{\gamma(s) :$*

$s \in [0, T)\}$ *as* $t \to \infty$.

We will denote the set of initial conditions for which trajectories converge to Γ as the basin of attraction (B.A.).

Definition 3 *The* <u>*phase*</u> *of a limit cycle with period* T *is a function* $\theta : \gamma \to S^1 = [0, 1)$ *such that*

$$\frac{d}{dt}\left(\theta(\gamma(t))\right) = 1/T, \tag{3}$$

where $\theta = 0$ *is chosen arbitrarily.*

Fig. 1.1 illustrates the relationship between a conductance-based model and the corresponding phase variable.

If the limit cycle is hyperbolic[1], then given a point $x_0 \in B.A.$, there exists a unique $\theta(x_0)$ such that

$$\lim_{t \to \infty} ||x(t) - \gamma(t + T\theta(x_0))|| \to 0. \tag{4}$$

Definition 4 *The value* $\theta(x_0)$ *in Eq. (4) is the* <u>*asymptotic phase*</u> *of the point* x_0.

---

[1]A hyperbolic limit cycle is such that the modulus of the Floquet multipliers corresponding to the eigenvectors transverse to the limit cycle are strictly less than unity [12].
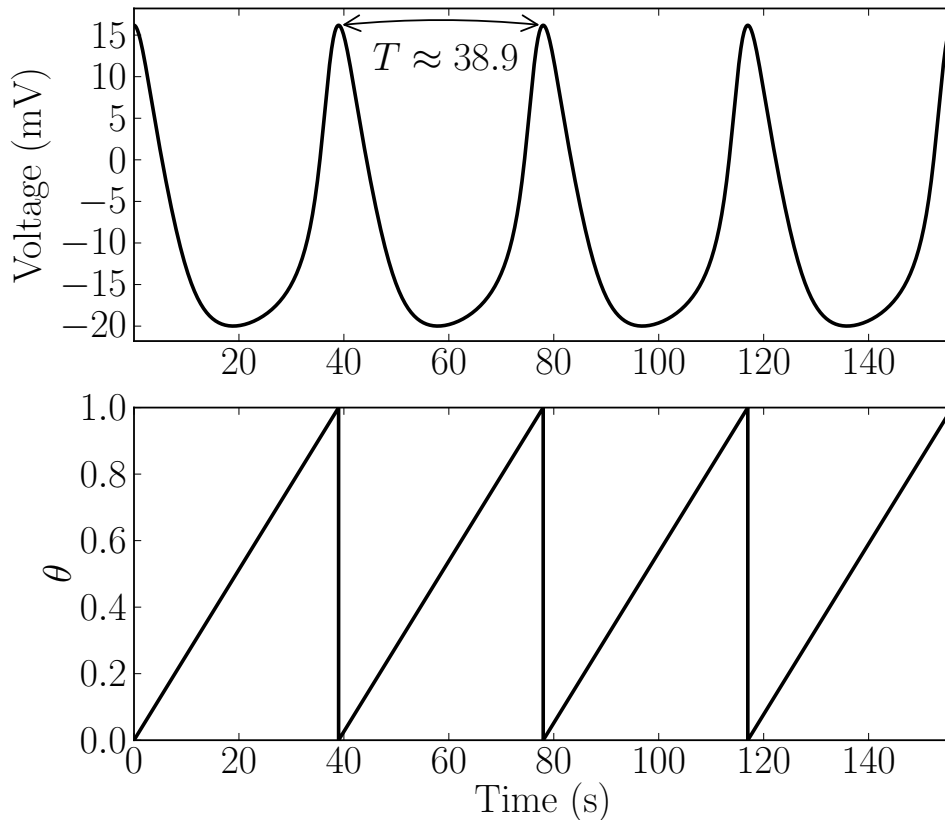
Figure 1.1: The phase function θ over time. The top panel is a voltage trace of a limit cycle of the Morris-Lecar model (defined in Appendix A.2.1). The bottom panel shows the corresponding phase values with respect to the limit cycle. Here, we have defined zero phase corresponding to peak voltage, as is typical with many neurobiological models.

By construction, the asymptotic phase function, $\theta(x)$, has the property that

$$\frac{d}{dt}\left(\theta(x(t))\right) = 1/T, \tag{5}$$

for any trajectory in B.A.

Definition 5 *An <u>isochron</u> is a level curve consisting of points that share the*

same asymptotic phase (Fig. 1.2). In other words, two points $x_0, x_1 \in B.A.$
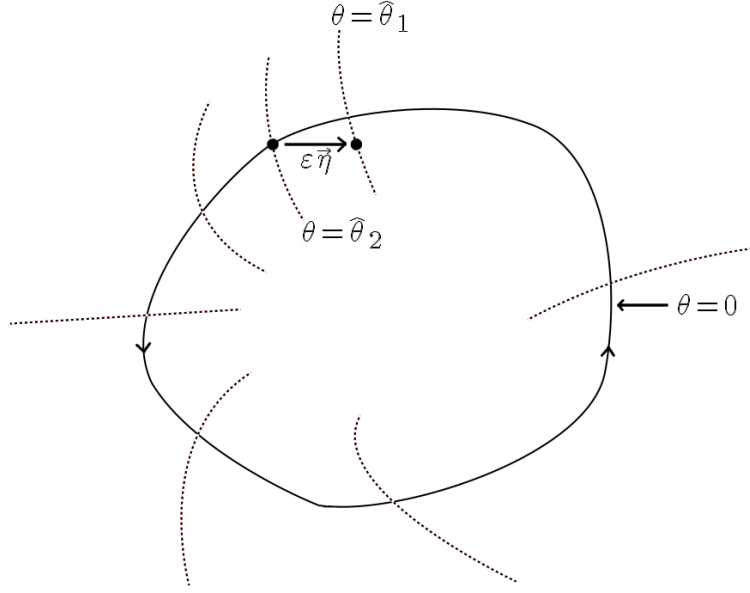
Figure 1.2: Isochrons of a planar limit cycle. Dashed lines represent isochrons, which are level curves of points sharing the same asymptotic phase. In this example, a small perturbation of size ε in direction η at phase $\hat{\theta}_2$ pushes a trajectory to a different isochron, leading to a phase shift of $\Delta\theta = \hat{\theta}_1 - \hat{\theta}_2$.

are on the same isochron if for two trajectories $\hat{x}_1$ and $\hat{x}_2$,

$$\lim_{t\to\infty} |\hat{x}_1(t) - \hat{x}_2(t)| = 0, \tag{6}$$

where the trajectories have initial conditions, $\hat{x}_1(0) = x_0$ and $\hat{x}_2(0) = x_1$.

The change in phase, $\Delta\theta$, in response to a perturbation of size ε in the unit

vector direction η, depends on the time at which the perturbation occurs. To

derive the infinitesimal phase response curve, provided the asymptotic phase

function θ is C^1, we expand the function to first order in ε.

$$\theta(\gamma(t) + \varepsilon\eta) = \theta(\gamma(t)) + \varepsilon D\theta(\gamma(t)) \cdot \eta + O(\varepsilon^2),$$

$$\Delta\theta = \theta(\gamma(t) + \varepsilon\eta) - \theta(\gamma(t)) = \varepsilon D\theta(\gamma(t)) \cdot \eta + O(\varepsilon^2), \qquad (7)$$

$$\lim_{\varepsilon \to 0} \frac{\Delta\theta}{\varepsilon} = D\theta(\gamma(t)) \cdot \eta =: z(t) \cdot \eta.$$

We define the gradient of the phase function, $D\theta(\gamma(t))$, to be the iPRC, $z(t)$. Explicit solutions exist for only a few cases (see Appendix A.4). The iPRC may be approximated by direct perturbations, or alternatively by solving an adjoint equation,

$$\frac{dz}{dt} = A(t)z(t), \qquad (8)$$

where $A(t) = -DF^T(\gamma(t))$, the negative transpose of the linearization of the vector field F evaluated along the limit cycle γ. See Appendix A.1 for a derivation of the equation.

1.2 Infinitesimal Phase Response Curves and Differential Inclusions

Differential inclusions are rigorously defined in [9]. Here we consider a simplified definition. Let $B \subset \mathbb{R}^n$ be path connected. A vector field $F : B \to \mathbb{R}^n$ is piecewise smooth on B if there exist a finite number, K, of open sets B_k such that

1. B_k is nonempty, simply connected, and open for each k.

2. $B_i \cap B_j = \varnothing, \forall i \neq j$.

3. $B \subset \bigcup_{k=1}^K \bar{B}_k$.

4. There exist smooth, bounded vector fields $F^k : \bar{B}_k \to \mathbb{R}^n$ such that for all x in B_k, $F^k(x) = F(x)$.

Note that we require $F^k = F$ only on the interior of each open domain B_k, while we require F^k be smooth on the closure $\bar{B}_k$. We also assume that the vector fields are arranged in such a way that a limit cycle exists. In the basin of attraction of the limit cycle, we further assume that vector fields F^k, F^{k+1} on adjacent sets B_k, B_{k+1}, "flow" in the same direction at the boundary $\bar{B}_k \cap \bar{B}_{k+1}$ within a subset of the basin of attraction (Fig. 1.3). Finally, we assume that there exists a neighborhood about the point γ^∂, within which the boundary is C^1. Later we will specialize to the case where each vector field is defined by a system of linear equations.

We now state several assumptions regarding limit cycles, phase, and isochrons.

1. *Existence and uniqueness holds for trajectories in the differential inclusions we consider.*

   Without giving a formal proof, we note that existence and uniqueness of trajectories holds within each domain B_k. By using the final coordinate
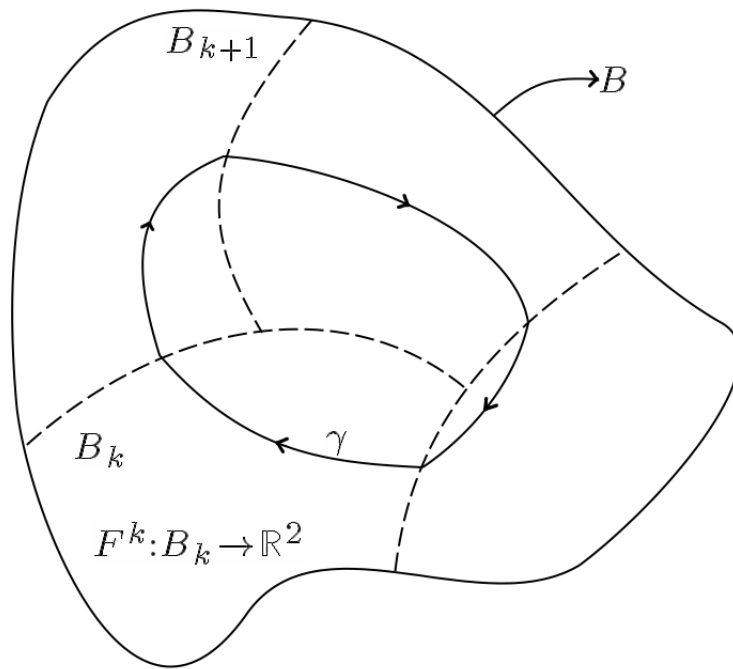
Figure 1.3: Example domains of a piecewise smooth dynamical system. Each domain is separated by dashed lines. A loop, γ, traversing all domains illustrates a limit cycle. See Figs. A.3 and A.2 for concrete examples of PWL models.

of a trajectory x^k in B_k as the initial condition of a trajectory x^{k+1} in B_{k+1}, we have the existence and uniqueness of the trajectory x^{k+1} because the vector field defined over B_{k+1} is smooth. It seems plausible that existence and uniqueness for typical trajectories passing through multiple domains would follow by induction.

2. *The system has a stable limit cycle with well-defined phase.*

   Given existence and uniqueness of trajectories, there exist piecewise smooth vector fields with well-defined, isolated, T-periodic orbits. The phase of a T-periodic limit cycle in a piecewise smooth dynamical sys-

tem follows naturally from the definition of phase, with $d\theta/dt = 1/T$. By "stable limit cycle", we also mean to assume that the limit cycle is in the interior of an open set contained in the basin of attraction.

3. *A unique asymptotic phase exists for all points in the basin of attraction.*

   Existence and uniqueness of the asymptotic phase would follow from the assumed existence and uniqueness of solutions in the basin of attraction.

4. *Isochrons exist and are continuous.*

   Continuity of isochrons is equivalent to continuity of the phase function. That is to say, for $x \in \Gamma$,

   $$\forall \varepsilon > 0, \exists \delta > 0 \text{ s.t. } y \in B(x, \delta) \Rightarrow ||\theta(x) - \theta(y)|| < \varepsilon. \tag{9}$$

   We further assume that the asymptotic phase function satisfies

   $$\frac{d\theta(x(t))}{dt} = 1/T, \quad \forall x(t) \in B.A. \tag{10}$$

5. $\theta(x)$ *is locally differentiable at each domain boundary, in the direction tangent to the boundary.* Generally, the asymptotic phase function will not necessarily be differentiable in the direction transverse to the boundary.

The definition of the iPRC does not apply directly to piecewise smooth differential equations. For instance, the adjoint equation (Eqs. 7 and 8) may

not be solvable over a finite collection of sets, because the Jacobian may be ambiguous at the boundaries. This problem of applying the adjoint equation to DIs has had limited attention. Shaw et al. (2012) produced exact results for the iPRC of the iris system (a PWL model defined in Appendix A.2.5) using a direct derivation, but the method does not apply to general piecewise linear systems. Coombes formulated a more general form for the iPRC of PWLDS and applied the theory to two planar PWL models [6]. However, this method does not hold in cases where the iPRC is discontinuous, as it is for the iris system. We now show how to solve for the iPRC for general planar piecewise smooth dynamical systems.

2 The Infinitesimal Phase Response Curve of Piecewise Smooth Dynamical Systems

2.1 Discontinuities of Infinitesimal Phase Response Curves of Differential Inclusions

Consider a DI as constructed in Section 1.2. The vector field along the limit cycle may be discontinuous along domain boundaries, leading to discontinuity in the iPRC. Our main result, Theorem 1, shows how to calculate these discontinuities. This expression, with the adjoint equation, constitute a complete picture of the iPRC of a DI.

We first fix notation and define terms before introducing the theorem. Let F^R denote the vector field of region R, where each region is numbered according to the direction of flow within a neighborhood of the limit cycle, and assuming trajectories enter or exit transverse to the boundary with respect to each region. The limit cycle, γ, is piecewise smooth, consisting of several curves $\gamma^1, \gamma^2, ...\gamma^K$. Each γ^R spends a total time t_R in its domain. We write the limit
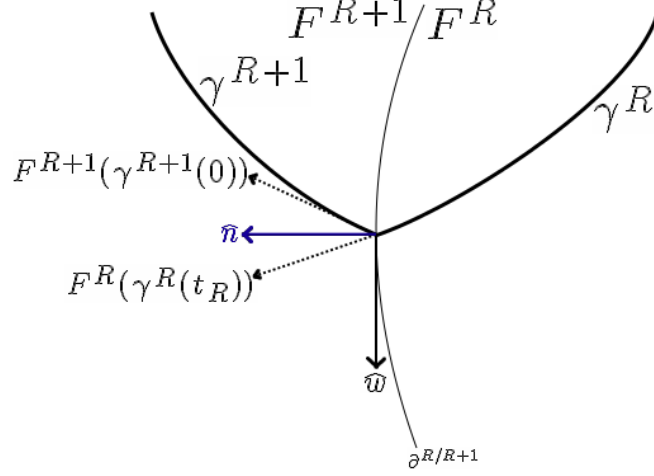
Figure 2.1: Piecewise smooth region setup and notation. The boundary separating the sets B^R and B^{R+1} (with vector fields F^R and F^{R+1}, respectively) is denoted by $\partial^{R/R+1}$. The limit cycle, γ, with solutions in region R and $R+1$ (denoted γ^R, γ^{R+1}, respectively) is continuous across the boundary. We use local time for γ^R and γ^{R+1} so that $\gamma^R(t_R) = \gamma^{R+1}(0)$, where t_R is the time of flight through region R (see Eq. (11)). The values $F^R(\gamma(t_R))$, $F^{R+1}(\gamma(t_R))$ is the vector field in region R, $R+1$ at the point of egress and ingress, respectively, with vector $\hat{n}$ normal to the boundary and $\hat{w}$ tangent to the boundary.

cycle γ as a collection of curves,

$$
\gamma(t) = \begin{cases} \gamma^1(t), & 0 = T_0 \le t < T_1, \\[2mm] \gamma^2(t - T_1), & T_1 \le t < T_2, \\[2mm] \vdots & \\[2mm] \gamma^K(t - T_{K-1}), & T_{K-1} \le t < T_K, \end{cases} \tag{11}
$$

where $T_i = \sum_{j=1}^{i} t_j$ and $\gamma^R(t_R) = \gamma^{R+1}(0)$. The final and initial values of two adjacent vector fields, F^R, F^{R+1}, along the limit cycle are denoted

$$
F_0^{R+1} = \lim_{t \to 0^+} F^{R+1}(\gamma^{R+1}(t)), \qquad\qquad F_f^R = \lim_{t \to t_R^-} F^R(\gamma^R(t)). \tag{12}
$$

In Eq. (12) and for the rest of the section, the value t is taken to be local, i.e. the time elapsed since entering the current region. The one-sided limits exist because each vector field is smooth on its domain. The iPRC, $z(t)$, will be represented segment-by-segment with similar notation. Define terms z_f^R and z_0^{R+1} by

$$z_f^R = \lim_{t \to t_R^-} z^R(t), \tag{13}$$

$$z_0^{R+1} = \lim_{t \to 0^+} z^{R+1}(t), \tag{14}$$

where z^R and z^{R+1} are the solutions to the adjoint equation in regions R and $R + 1$, respectively. Let ψ_R be the angle of the vector normal to the boundary (with respect to a global Cartesian coordinate system) at which the limit cycle crosses the boundary. Call this crossing point γ^∂. Finally, let $\hat{n} = (\cos \psi_R, \sin \psi_R)$ denote the unit vector normal to the boundary at γ^∂, and let $\hat{w} = (-\sin \psi_R, \cos \psi_R)$ denote the unit vector tangent to the boundary at γ^∂ (see Fig. 2.1). We now introduce the theorem.

Theorem 1 *Let γ be a piecewise smooth limit cycle in $\mathbb{R}^2$ satisfying assumptions $1 - 5$ in Section 1.2. The iPRC for γ satisfies the following boundary condition at the boundary $\partial^{R/R+1}$,*

$$z_0^{R+1} = M^R z_f^R, \tag{15}$$

where

$$M^R = \begin{pmatrix} f_0^{R+1} & g_0^{R+1} \\ -\sin\psi_R & \cos\psi_R \end{pmatrix}^{-1} \begin{pmatrix} f_f^R & g_f^R \\ -\sin\psi_R & \cos\psi_R \end{pmatrix}. \tag{16}$$

Existence of the required matrix inverse is guaranteed by the transverse flow condition, $F_0^{R+1} \cdot \hat{n} > 0$.

Proof Recall that we assign asymptotic phase values $\theta(x)$ for points in the stable limit cycle Γ, and in its basin of attraction, B.A. The asymptotic phase function, θ, is differentiable in the interior of each region and remains continuous at the boundaries. The phase function is not necessarily differentiable on the boundaries with respect to space, but θ is always differentiable as a function of time, since we assume $d\theta(x(t))/dt = 1/T$ for any trajectory $x(t)$ in the basin of attraction.

These assumptions allow us to derive two linear equations satisfied by the iPRC, z, at each boundary. Suppose we are at an arbitrary boundary between regions R and $R+1$ (denoted $\partial^{R/R+1}$). We denote the iPRC in regions R and $R+1$ by z^R, z^{R+1}, respectively. By the chain rule, for $k \in \{R, R+1\}$, we have the useful relation,

$$\frac{d\theta}{dt} = F^k(x^k(t)) \cdot \nabla\theta(x^k(t)). \tag{17}$$

When $x^k(t) = \gamma^k(t)$, we have (by definition)

$$\frac{d\theta}{dt} = F^k(\gamma^k(t)) \cdot z^k(t). \tag{18}$$

Recall that $d\theta/dt = 1/T$. By taking the one-sided limits

$$\lim_{t \to t_R^-} F^R(\gamma^R(t)) \cdot z^R(t) = F_f^R \cdot z_f^R,$$

$$\lim_{t \to 0^+} F^{R+1}(\gamma^{R+1}(t)) \cdot z^{R+1}(t) = F_0^{R+1} \cdot z_0^{R+1},$$

(19)

we have the first equation relating z^R and z^{R+1},

$$F_f^R \cdot z_f^R = \frac{1}{T} = F_0^{R+1} \cdot z_0^{R+1}.$$

(20)

Intuitively, Eq. (20) states that the phase function advances at the same rate as a function of time everywhere, and in particular on both sides of the boundary $\partial^{R/R+1}$, so the limits in Eq. 19 must be equal.

To derive the second equation relating z^R and z^{R+1}, we recall that the isochrons are continuous along each boundary, by assumption. Define a coordinate, w, along the boundary such that the limit cycle crosses at $w = 0$. For some interval $w_{\min} < 0 < w_{\max}$, w represents a point on the intersection of the boundary in B.A. For any such point w, we can write the limit of the asymptotic phase function, θ^k, from region $k \in \{R, R+1\}$, respectively, to the boundary as $\theta^k(w)$. However, because isochrons are continuous across the boundary,

$$\theta^R(w) = \theta^{R+1}(w).$$

(21)

Moreover, by assumption, the partial derivatives of the isochrons with respect

to w coincide at the boundary, so

$$\frac{d\theta^R}{dw}(w) = \frac{d\theta^{R+1}}{dw}(w), \tag{22}$$

for any value of $w \in (w_{\min}, w_{\max})$. We can rewrite an equivalent expression using the directional derivative,

$$\left(\nabla\theta^R(w)\right) \cdot \hat{w} = \left(\nabla\theta^{R+1}(w)\right) \cdot \hat{w}. \tag{23}$$

In particular, for $w = 0$,

$$z^R(t_R) \cdot \hat{w} = z^{R+1}(0) \cdot \hat{w}, \tag{24}$$

which gives us our second equation,

$$z_f^R \cdot \hat{w} = z_0^{R+1} \cdot \hat{w}. \tag{25}$$

We can combine equations (20) and (25) and rearrange as a system of equations,

$$\begin{pmatrix} f_0^{R+1} & g_0^{R+1} \\ -\sin\psi_R & \cos\psi_R \end{pmatrix} z_0^{R+1} = \begin{pmatrix} f_f^R & g_f^R \\ -\sin\psi_R & \cos\psi_R \end{pmatrix} z_f^R. \tag{26}$$

The theorem follows upon left-multiplying the system by the inverse of the

matrix on the left-hand side. We are guaranteed invertibility as long as

$$\det \begin{pmatrix} f_0^{R+1} & g_0^{R+1} \\ -\sin\psi_R & \cos\psi_R \end{pmatrix} \neq 0. \tag{27}$$

But by assumption, $\det \begin{pmatrix} f_0^{R+1} & g_0^{R+1} \\ -\sin\psi_R & \cos\psi_R \end{pmatrix} = F_0^{R+1} \cdot \hat{n} > 0.$ ∎

We now focus on piecewise linear differential equations.

Corollary 2 *With the assumptions of Theorem 1 and affine linear vector fields F^k, the initial condition of the iPRC, $z(t)$, must satisfy*

$$z_0^1 = B z_0^1, \tag{28}$$

where

$$B = M^K e^{A^K t_K} \cdots M^1 e^{A^1 t_1}, \tag{29}$$

t_k is the time of flight through the kth region, e^{A^k} is the matrix exponential of $A^k = -\left(DF^k\right)^\mathsf{T}$. Eq. (28) and the normalization condition,

$$F_0^1 \cdot z_0^1 = \frac{1}{T}, \tag{30}$$

yield a unique solution for the initial condition, $z_0^1 \in \mathbb{R}^2$, provided the nullspace of the matrix $B - I$ does not have dimension greater than one.

Proof Let z_0^1 be the initial condition for the adjoint equation, and let $z_i^1(0)$ be the ith component. To prove the corollary, we solve the adjoint equation for region R, apply the matrix M^R at the boundary to calculate jumps in the iPRC, then repeat the process for region $R+1$ and continue inductively for subsequent regions.

Beginning with an arbitrary region, which we label $R = 1$, the solution at t_1 (the time of flight through region $R = 1$), is

$$z_f^1 = e^{A^1 t_1} z_0^1, \tag{31}$$

where $A(t) = -DF^T(\gamma(t))$ is constant. The initial condition for the next region, z_0^2, is equal to the final value of the previous region with jumps calculated by M^1,

$$z_0^2 = M^1 e^{A^1 t_1} z_0^1. \tag{32}$$

We can continue this procedure inductively for the initial condition of the Kth iPRC,

$$z_0^K = M^{K-1} e^{A^{K-1} t_{K-1}} \cdots M^1 e^{A^1 t_1} z_0^1. \tag{33}$$

Since the underlying limit cycle is periodic, $z(t)$ must be periodic, therefore $z^{K+1}(0) = z^1(0)$, and

$$z_0^1 = M^K e^{A^K t^K} M^{K-1} e^{A^{K-1} t^{K-1}} \cdots M^1 e^{A^1 t^1} z_0^1. \tag{34}$$

The first statement in the corollary follows upon collapsing the matrix product

into a 2×2 matrix B.

To prove uniqueness, we follow a procedure similar to that used in [6] and

apply Eqs. (28) and (30). Rewriting Eq. (28),

$$
\begin{pmatrix} z_1^1(0) \\ z_2^1(0) \end{pmatrix} = z_0^1 = B z_0^1
$$

$$
= \begin{pmatrix} b_{11} z_1^1(0) + b_{12} z_2^1(0) \\ b_{21} z_1^1(0) + b_{22} z_2^1(0) \end{pmatrix}. \tag{35}
$$

we can rewrite Eq. (35) as a system of equations for $z_1^1(0)$ and $z_2^1(0)$,

$$
z_1^1(0)(1 - b_{11}) = b_{12} z_2^1(0),
$$

$$
z_2^1(0)(1 - b_{22}) = b_{21} z_1^1(0). \tag{36}
$$

Without loss of generality, we choose the first of Eq. (35) combined with

Eq. (30) to form the system of equations,

$$
z_1^1(0) f_0^1 + z_2^1(0) g_0^1 = \frac{1}{T},
$$

$$
z_1^1(0)(b_{11} - 1) + b_{12} z_2^1(0) = 0, \tag{37}
$$

which we solve by inverting the matrix in the equivalent equation,

$$
\begin{pmatrix} f_0^1 & g_0^1 \\ (b_{11} - 1) & b_{12} \end{pmatrix} \begin{pmatrix} z_1^1(0) \\ z_2^1(0) \end{pmatrix} = \begin{pmatrix} \frac{1}{T} \\ 0 \end{pmatrix},
\tag{38}
$$

which establishes uniqueness of the solution, provided

$$
\det \begin{pmatrix} f_0^1 & g_0^1 \\ (b_{11} - 1) & b_{12} \end{pmatrix} \neq 0.
\tag{39}
$$

From the periodicity of the solution $z(t)$, we know that B has at least one eigenvector with unit eigenvalue. The condition (39) is equivalent to requiring that the matrix $B - I$ have a null space of not greater than one dimension. ∎

Corollary 3 *Under the assumptions of Corollary 2, if adjacent vector fields evaluated along the limit cycle, F_f^R and F_0^{R+1}, are continuous at the boundary $\partial^{R/R+1}$, then the matrix M^R is the identity.*

Proof Recall the form of the matrix M^R from Theorem 1,

$$
M^R = \begin{pmatrix} f_0^{R+1} & g_0^{R+1} \\ -\sin\psi_R & \cos\psi_R \end{pmatrix}^{-1} \begin{pmatrix} f_f^R & g_f^R \\ -\sin\psi_R & \cos\psi_R \end{pmatrix}.
\tag{40}
$$

If the vector fields on the limit cycle, F_f^R, F_0^{R+1} are C^0 (they agree at the

boundary), then

$$f_f^R = f_0^{R+1},$$

$$g_f^R = g_0^{R+1},$$

(41)

and the matrix product in Eq. (40) reduces to the identity matrix.

2.2   Applications

2.2.1   Piecewise Linear Morris-Lecar

The Morris-Lecar model is a conductance-based planar neurobiological model developed to understand oscillations in barnacle muscle fiber [16] (see Appendix A.2.1). In [6], Coombes constructed a piecewise linear approximation to the Morris-Lecar model for use in gap junction coupled networks (see Appendix A.2.3). Coombes provides an ad-hoc derivation of the iPRC, implicitly taking the matrix M^R to be the identity for each boundary crossing. Here we apply Corollary 3 and show that M^R is indeed the identity for all boundaries.

Let the piecewise linear Morris-Lecar be defined as in Appendix A.2.3. The model contains three distinct vector fields, separated by vertical gray lines in Fig. A.2. In the parameter regime we consider, the limit passes through the two rightmost boundaries, at $v = b = 0.5$ and $v = (1+a)/2 = 0.625$ (see Table A.2.3 for parameter values).

Along the boundary at $v = 0.5$, the first component, of the vector field, $\dot{v} = (f(v) - w + I)/C$, does not change over the boundary, so the first component agrees on both sides. However, the second component of the vector field changes and each side is by definition,

$$
g(v, w) = \begin{cases} (v - \gamma_1 w + b^* \gamma_1 - b)/\gamma_1, & v < b \\ (v - \gamma_2 w + b^* \gamma_2 - b)/\gamma_2, & v \geq b \end{cases}
$$

Let g^4 and g^1 denote the second component of the vector field to the left and right of the boundary. Along the boundary, $v = b$, so the difference in the vector fields at the boundary is

$$
g^4(b, w) - g^1(b, w) = (-\gamma_1 w + b^* \gamma_1)/\gamma_1 - (-\gamma_2 w + b^* \gamma_2)/\gamma_2
$$

$$
= 0.
$$

$$(42)$$

Therefore, the vector field agrees on both sides at the boundary for all points along the boundary. In particular, the vector field evaluated along any limit cycle is continuous at the boundary, so M^R is the identity by Corollary 3.

We observe similar behavior at the boundary $v = 0.625$. By definition, the second component of the vector field remains invariant when $v = 0.625$, while

the first component of the vector field changes over this boundary,

$$f(v) = \begin{cases} -v, & v < a/2 \\ v - a, & a/2 \leq v \leq (1+a)/2 \\ 1 - v, & v > (1+a)/2 \end{cases} , \tag{43}$$

where $\dot{v} = (f(v) - w + I)/C$. We consider f alone, since other parameters remain the same over the boundary. Let f^1 and f^2 denote the first component to the left and right of the boundary. The difference $f^1 - f^2$ is

$$f^1\left((1+a)/2, w\right) - f^2\left((1+a)/2, w\right) = (1+a)/2 - a - (1 - (1+a)/2)$$
$$\tag{44}$$
$$= 0.$$

Again, the vector fields evaluated along any limit cycle agree at the boundary, so the matrix M^R is the identity by Corollary 3.

Since the matrix M^R is the identity for each boundary crossing of the limit cycle, the iPRC is continuous (though not necessarily C^1). See Fig. 2.2 for the numerical iPRC that confirms this result.

2.2.2   McKean Model

The McKean model is a piecewise linear approximation to the FitzHugh-Nagumo model [13]. Let the McKean model be defined as in Appendix A.2.2. We use similar methods as in the previous section.

Figure 2.2: Numerical iPRCs of the PML system. Blue: perturbations in the positive horizontal direction. Gray: perturbations in the positive vertical direction. There are no discontinuities in either iPRC [6]. Copyright © 2008 Society for Industrial and Applied Mathematics. Reprinted with permission. All rights reserved.

The limit cycle for the McKean model passes through both boundaries, at $v = a/2 = 0.125$ and $v = (1 + a)/2 = 0.625$ (see Fig. A.1 and Table A.2.3 for parameter values). The second component of the vector field is invariant over each boundary, so we consider just the function f in the first component, $\dot{v} = (f(v) - w + I)/C$, since f is the only term that changes at the boundaries.

At the leftmost boundary, $v = 0.125$, the difference in the function f is,

$$-v|_{v=a/2} - (v - a)|_{v=a/2} = 0. \tag{45}$$

At the rightmost boundary, $v = 0.625$, the difference in the function f is,

$$(v - a)|_{v=(1+a)/2} - (1 - v)|_{v=(1+a)/2} = 0. \tag{46}$$

The vector field agrees on both sides at each boundary (and for vector fields evaluated along limit cycles in particular), so by Corollary 3, the matrix M^R is the identity for each boundary crossing.
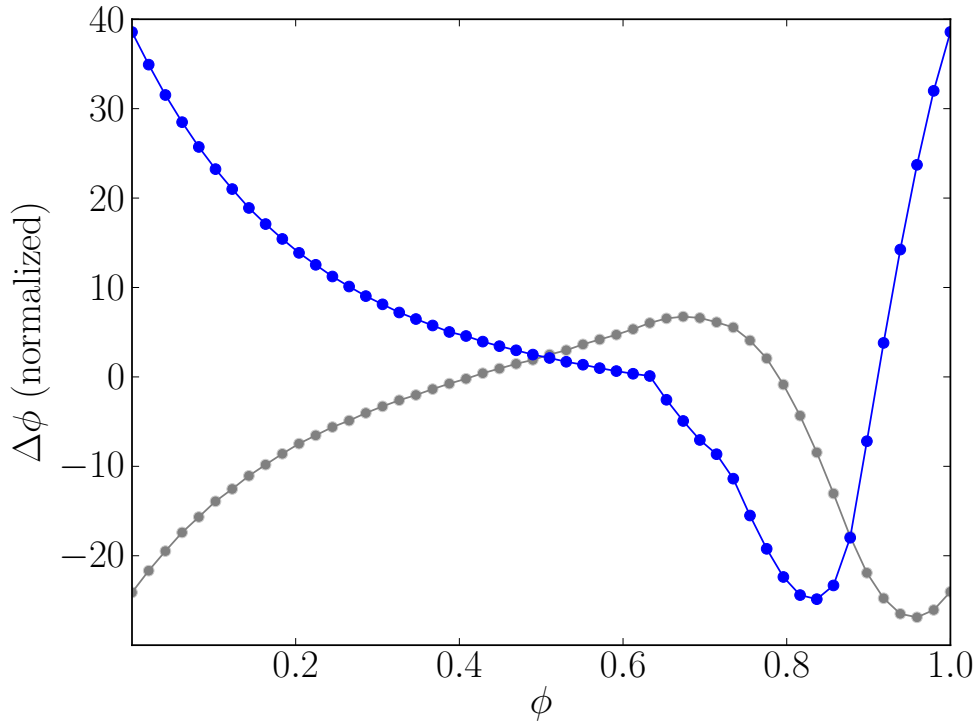

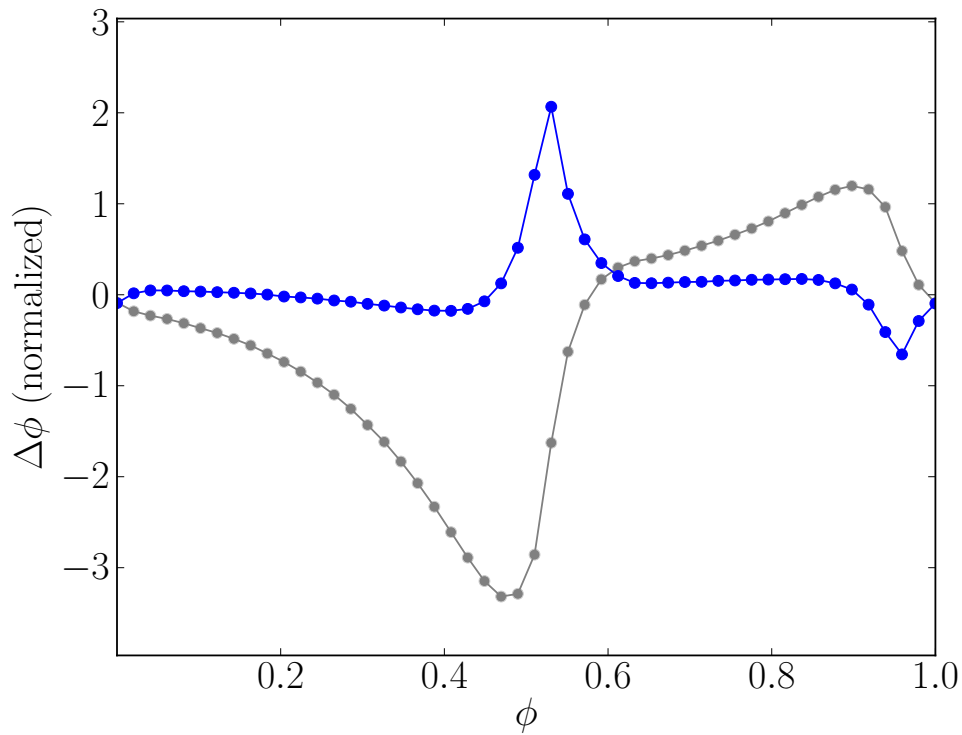Figure 2.3: Numerical iPRCs of the McKean model. Blue: perturbations in the positive horizontal direction. Gray: perturbations in the positive vertical direction. There are no discontinuities in either iPRC [6]. Copyright © 2008 Society for Industrial and Applied Mathematics. Reprinted with permission. All rights reserved.

Again, the iPRCs of both coordinates are continuous (but not necessarily C^1).

See Fig. 2.3 for the numerical iPRC that confirms this result. We direct the reader to [6] for explicit expressions of the iPRC of the PML and McKean models.

2.2.3 Iris System

The iris system is a piecewise linear dynamical system developed by Shaw et al. as an approximation to a particular smooth system, defined in Appendix A.2.4. This smooth system, which Shaw et al. referred to as the sine system, was constructed to explore the effects of changing trajectories to pass closer to or further from saddle points by changing a single parameter. Both the sine system and iris system exhibit a family of limit cycles, indexed by a single parameter, which undergo a bifurcation to a heteroclinic cycle as the parameter goes to zero [20]. Let the iris system be as defined in Appendix A.2.5. When the corresponding bifurcation parameter, a, for the iris system, is small and positive, the iris system also produces a stable limit cycle (Fig. A.3). The limit cycle enters the Southwest region at coordinates $(1, u)$ and exits at coordinates $(s, 1) = (u^\lambda, 1)$, with transit time $T = \log(1/u)$, and enters the next region at local coordinates $(1, s + a) = (1, u)$. Due to the symmetry of the iris system, the entry and exit coordinates of the other three regions are related by a 90-degree clockwise rotation, with each region having the same time of flight T. We define the phase $\theta = t/T$ for each region. As $a \to 0^+$, $u \to 0^+$, and the period T diverges.

The dynamics in each square of the iris system is defined by a system of decoupled linear differential equations. Therefore the Jacobian is a constant diagonal matrix, so the matrix exponential solution to the adjoint equation (Eq. 8) is diagonal. To solve for the initial conditions of the iPRC of the iris system, we use Corollary 2. First we obtain the matrix B by solving the adjoint equation up to the time of flight beginning with the Southwest (SW) region, applying Theorem 1 at the boundary between the SW and NW regions, then repeating inductively for the remaining three regions. We solve for the initial conditions of the iPRC in the SW region using Corollary 2. The iPRC of the SW region is equivalent to the iPRC for the remaining regions up to rotation.

Let (s, u) denote the local coordinates within an iris square, and (x, y) denote the global coordinates of the iris system. In each region the global coordinates differ from local coordinates by an affine rotation. Consider the boundary between the SW and NW squares. The dynamics in the SW square is

$$F^{SW} = \begin{pmatrix} dx/dt \\ dy/dt \end{pmatrix} = \begin{pmatrix} -\lambda(x + c_{SW}) \\ y + d_{SW} \end{pmatrix} = \begin{pmatrix} -\lambda s \\ u \end{pmatrix}, \tag{47}$$

where the constants c_{SW} and d_{SW} offset the vector field. The initial and final conditions of the vector field F^{SW} evaluated along a limit cycle γ with entry

coordinates at $(1, u)$ and exit coordinates $(s, 1)$, are

$$F_0^{SW} = (-\lambda, u)^T,$$
$$F_f^{SW} = (-\lambda s, 1)^T. \tag{48}$$

Its Jacobian is diagonal,

$$J_{SW} = \begin{pmatrix} -\lambda & 0 \\ 0 & 1 \end{pmatrix}, \tag{49}$$

and the solution to the adjoint equation, evaluated at the time of flight, is

$$z^{SW}(T) = \begin{pmatrix} e^{\lambda T} & 0 \\ 0 & e^{-T} \end{pmatrix} z^{SW}(0). \tag{50}$$

To obtain the jump condition matrix M^R between SW and NW, we need to write the vector field of the next square, which is related to the SW square by 90-degree rotation,

$$F^{NW} = \begin{pmatrix} dx/dt \\ dy/dt \end{pmatrix} = \begin{pmatrix} x + c_{NW} \\ -\lambda(y + d_{NW}) \end{pmatrix} = \begin{pmatrix} u \\ -\lambda s \end{pmatrix}, \tag{51}$$

where c_{NW} and d_{NW} offset the vector field F^{NW} and s and u are the (rotated) local coordinates. The initial and final vectors of F^{NW} along a limit cycle with the same entry and exit coordinates as before is related by the 90-degree

rotation matrix, $\mathcal{R} = \begin{pmatrix} 0 & 1 \\ -1 & 0 \end{pmatrix}$. Applying the rotation matrix to F^{NW} returns the initial and final coordinates for F^{NW} evaluated along the limit cycle,

$$F_0^{NW} = \mathcal{R}F_0^{SW} = (u, \lambda)^T,$$
$$F_f^{NW} = \mathcal{R}F_f^{SW} = (1, \lambda s)^T. \tag{52}$$

The Jacobian is

$$J_{NW} = \begin{pmatrix} 1 & 0 \\ 0 & -\lambda \end{pmatrix}, \tag{53}$$

and the solution to the adjoint evaluated at the time of flight is

$$z^{NW}(T) = \begin{pmatrix} e^{-T} & 0 \\ 0 & e^{\lambda} \end{pmatrix} z^{NW}(0). \tag{54}$$

By Theorem 1,

$$M^{SW} = \begin{pmatrix} u & \lambda \\ -1 & 0 \end{pmatrix}^{-1} \begin{pmatrix} -\lambda s & 1 \\ -1 & 0 \end{pmatrix}$$
$$= \begin{pmatrix} -1 & 0 \\ s + \frac{u}{\lambda} & -\frac{1}{\lambda} \end{pmatrix}. \tag{55}$$

So across the boundary,

$$
\begin{aligned}
z_0^{NW} &= \begin{pmatrix} -1 & 0 \\ s + \frac{u}{\lambda} & -\frac{1}{\lambda} \end{pmatrix} z_f^{SW}. \\
&= \begin{pmatrix} -1 & 0 \\ s + \frac{u}{\lambda} & -\frac{1}{\lambda} \end{pmatrix} \begin{pmatrix} e^{\lambda T} & 0 \\ 0 & e^{-T} \end{pmatrix} z_0^{SW},
\end{aligned}
\tag{56}
$$

In the Northeast (NE) square, the dynamics are,

$$
F^{NE} = \begin{pmatrix} dx/dt \\ dy/dt \end{pmatrix} = \begin{pmatrix} -\lambda(x + c_{NE}) \\ (y + d_{NE}) \end{pmatrix} = \begin{pmatrix} -\lambda s \\ u \end{pmatrix},
\tag{57}
$$

where c_{NE}, d_{NE} are the constants offsetting the vector field in the NE square, and s and u are local coordinates within the NE square. Note that in terms of the local coordinates, F^{NE} and F^{SW} have the same form, consistent with the rotational symmetry of the system. The initial and final values of the vector field F^{NE} evaluated along the limit cycle is related by a 90-degree rotation,

$$
\begin{aligned}
F_0^{NE} &= \mathcal{R} F_0^{NW} = (\lambda, -u)^T, \\
F_f^{NE} &= \mathcal{R} F_f^{NW} = (\lambda s, -1)^T.
\end{aligned}
\tag{58}
$$

The Jacobian is the same as in the SW square, so the solution to the adjoint

is identical, with different initial conditions. By Theorem 1,

$$
\begin{aligned}
M^{NW} &= \begin{pmatrix} \lambda & -u \\ 0 & 1 \end{pmatrix}^{-1} \begin{pmatrix} 1 & \lambda s \\ 0 & 1 \end{pmatrix} \\
&= \begin{pmatrix} \frac{1}{\lambda} & s + \frac{u}{\lambda} \\ 0 & 1 \end{pmatrix}.
\end{aligned}
\tag{59}
$$

The adjoint now consists of a product of four matrices,

$$
\begin{aligned}
z_0^{NE} &= \begin{pmatrix} \frac{1}{\lambda} & s + \frac{u}{\lambda} \\ 0 & 1 \end{pmatrix} \begin{pmatrix} e^{\lambda T} & 0 \\ 0 & e^{-T} \end{pmatrix} z_0^{NW} \\
&= \begin{pmatrix} \frac{e^{(\lambda-1)T}}{\lambda} - e^{2\lambda T}\left(\frac{u}{\lambda} + s\right)^2, & \frac{e^{(\lambda-1)T}}{\lambda}\left(\frac{u}{\lambda} + s\right) \\ e^{2\lambda T}\left(-\frac{u}{\lambda} - s\right), & \frac{e^{(\lambda-1)T}}{\lambda} \end{pmatrix} z_0^{SW}.
\end{aligned}
\tag{60}
$$

The remaining jump matrices for the Northeast (NE) and Southeast (SE) squares, M^{NE} and M^{SE}, are identical to the SW and NW squares, respectively. Similarly, the Jacobian matrices of the NE and SE squares are the same as the corresponding matrices of the SW and NW squares. Therefore the matrix B of Corollary 2 is obtained by repeating the product of four matrices above,

$$
\begin{aligned}
z_0^{SW} &= B z_0^{SW} \\
&= \begin{pmatrix} \frac{e^{(\lambda-1)T}}{\lambda} - e^{2\lambda T}\left(\frac{u}{\lambda} + s\right)^2, & \frac{e^{(\lambda-1)T}}{\lambda}\left(\frac{u}{\lambda} + s\right) \\ e^{2\lambda T}\left(-\frac{u}{\lambda} - s\right), & \frac{e^{(\lambda-1)T}}{\lambda} \end{pmatrix}^2 z_0^{SW}.
\end{aligned}
\tag{61}
$$

Recalling that $e^{-T} = u$, and $e^{\lambda T} = 1/s$, it is straightforward to check that the

matrix B has an eigenvector $(s,1)^T$ with unit eigenvalue, so the initial condition of the iPRC is proportional to this vector, $z_0^{SW} \propto (s,1)^T$. By Corollary 2, the normalization condition $z_0^{SW} \cdot F_0^{SW} = 1/T$ determines the length of the vector z_0^{SW}.

Recalling that $s = u^\lambda$, in the SW square, $F_0^R = (-\lambda, u)^T$, so

$$
\begin{aligned}
z_0^{SW} \cdot F_0^{SW} &= s(-\lambda) + u \\
&= u - \lambda u^\lambda.
\end{aligned}
\tag{62}
$$

Therefore, in order for $z_0^{SW} = (s,1)$ to satisfy the normalization condition, it must be scaled by the value $\frac{1}{T(u-\lambda u^\lambda)}$, which gives us our initial condition,

$$
z_0^{SW} = \left(\frac{u^\lambda}{T(u - \lambda u^\lambda)}, \frac{1}{T(u - \lambda u^\lambda)} \right).
\tag{63}
$$

Combining this expression with the solution to the adjoint equation, $z(t)^{SW}$, and recalling that $t = \theta T = \theta \log(1/u)$, yields

$$
\begin{aligned}
z^R(t) &= \begin{pmatrix} e^{\lambda t} & 0 \\ 0 & e^{-t} \end{pmatrix} z_0^R \\
&= \begin{pmatrix} e^{\lambda \theta T} & 0 \\ 0 & e^{-\theta T} \end{pmatrix} \begin{pmatrix} \frac{u^\lambda}{T(u-\lambda u^\lambda)} \\ \frac{1}{T(u-\lambda u^\lambda)} \end{pmatrix} \\
&= \begin{pmatrix} \frac{u^{\lambda(1-\theta)}}{T(u-\lambda u^\lambda)} \\ \frac{u^\theta}{T(u-\lambda u^\lambda)} \end{pmatrix}.
\end{aligned}
\tag{64}
$$

Expression (64)is exactly the iPRC derived in [20]. This alternative derivation is greatly simplified compared to the direct derivation in [20], which involved the laborious task of keeping track of perturbed trajectories over an infinite series of boundary crossings. In contrast, Theorem 1 requires relatively simple calculations involving the vector fields, limit cycle, and adjoint equation, and extends naturally to general piecewise smooth dynamical systems.

3 Discussion and Conclusions

The infinitesimal phase response curve provides insight into how CPGs adaptively respond to perturbations including mechanical loads and sensory feedback. Traditional CPG models are smooth, and the iPRC is obtained by numerically integrating the adjoint equation. However, standard methods for obtaining the iPRC fail for flows with discontinuous vector fields. We overcome this problem by deriving a boundary condition that allows integration of the adjoint equation around the limit cycle for such systems. In the case of piecewise linear dynamics, this approach can lead to analytically exact expressions for the iPRC. Theorem 1 provides a concise way to calculate an important portion of the iPRC for general planar DIs satisfying the assumptions in Section 1.2, and improves upon two known methods for calculating the iPRC of DIs.

We did not cover a general method to solve the adjoint equation (Eq. 8) within

each piecewise linear domain because methods for solving coupled systems of linear differential equations are known. In [6], the coupled linear differential equations are solved by diagonalizing a matrix exponential, which provides an explicit form for the matrix A in Eq. (8). In the iris system, both state variables are decoupled, so solving for the adjoint is a matter of solving two separate linear differential equations and taking advantage of the special symmetry to derive a unique solution. In [20] the iPRC was obtained through analysis of an infinite series capturing the compounded effects of offsets in position and time. The method used by Shaw et al. would become intractable if applied to a system with different saddle values, λ_i, in each domain of the system. For our method, by contrast, naturally includes systems in which the linear vector fields are not related by rotational symmetry, thereby providing a more flexible method for deriving the iPRC. For nonlinear dynamics, the adjoint equation may be solved numerically, by taking advantage of our jump condition.

Generalized iPRCs with periodic or random perturbations are beyond the scope of this discussion. However, it is worth noting that if a limit cycle is strongly attracting, then the iPRC may be used to calculate the response of the system to either periodic or random perturbations.

There are numerical advantages to our method as well. The iPRC for a DI (and indeed for any system with a limit cycle) is traditionally derived by perturbing a limit cycle in phase space and tracking the asymptotic change in phase. This direct simulation, while providing an accurate approximation to the iPRC, can

be computationally expensive. For example, one must evaluate a perturbed trajectory for several limit cycle periods to approximate the asymptotic phase, and one must repeat this calculation as many as one hundred times. By using the theorem, the iPRC can be solved with as little as two limit cycle evaluations, one to find the period and limit cycle trajectory, and the other to solve the adjoint equation over each piecewise smooth region.

The main result of this thesis should prove useful in the continued use of piecewise smooth dynamical systems and phase response curves in mathematical biology. Research in coupled oscillators has typically been restricted to smooth systems, or piecewise linear systems [6]. Our result allows for the possibility for using a broader class of dynamical systems to study biological oscillators. Finally, it is possible to derive exact expressions for the iPRC resulting from mechanical perturbations using piecewise linear dynamical systems.

In future work, we plan to extend the results of this thesis to n dimensions. The tools for smooth systems and many of our assumptions for piecewise smooth dynamical systems apply in n-dimensions. Derivation of the matrix M^R may include similar proof techniques.

A Appendix

A.1 Adjoint Equation

In this section we give an informal derivation of the adjoint equation satisfied by the infinitesimal phase response curve for a limit cycle in a smooth system of differential equations $dx/dt = F(x)$, introduced in Eq. (7), namely:

$$\frac{dz}{dt} = A(t)z(t), \tag{65}$$

where $A(t) = -DF^T(x(t))$, and $z(t) = \nabla\theta(x(t))$. For a more detailed proof, see [2] or [8]. Recall that

$$\frac{d\theta}{dt} = \frac{1}{T}. \tag{66}$$

Then

$$\begin{aligned}
0 &= \frac{d}{dt}\left(\frac{d\theta}{dt}\right) \\
&= \frac{d}{dt}\left(\nabla\theta(x(t)) \cdot \frac{dx}{dt}\right) \\
&= \left(\frac{d}{dt}\nabla\theta(x(t))\right) \cdot \frac{dx}{dt} + \nabla\theta \cdot \left(DF(x(t))\frac{dx}{dt}\right) \\
&= \left(\frac{d}{dt}\nabla\theta(x(t))\right) \cdot \frac{dx}{dt} + DF^T(x(t))\nabla\theta \cdot \frac{dx}{dt} \\
&= \left[\frac{d}{dt}\nabla\theta(x(t)) + DF^T(x(t))\nabla\theta(x(t))\right] \cdot F(x(t)).
\end{aligned} \tag{67}$$

We assume that $F(x(t)) \neq 0$ and that the dot product in the last line of

Eq. (67) does not reduce to zero, so

$$\frac{d}{dt}\nabla\theta(x(t)) + DF^T(x(t))\nabla\theta(x(t)) = 0$$

$$\Leftrightarrow \frac{d}{dt}\nabla\theta(x(t)) = -DF^T(x(t))\nabla\theta(x(t)). \tag{68}$$

When $x(t)$ is taken to be on the limit cycle, we recover the adjoint equation,

$$\frac{dz}{dt} = -DF^T(\gamma(t))z(t). \tag{69}$$

A.2   Model Equations

In this section we provide, as a reference, the model equations for various systems discussed in the main text.

A.2.1   Morris-Lecar

One well-studied neurobiological model capable of producing oscillatory behavior is the Morris-Lecar model. The model was developed by Cathy Morris and Harold Lecar in 1981 to describe the many oscillations in barnacle muscle fiber [16]. It is a conductance-based model with two state variables, so one may think of the model as a simplified model of Hodgkin-Huxley type. The

equations for the Morris-Lecar system are as follows:

$$C\frac{dV}{dt} = I - g_L(V - E_L) - g_k n(V - E_K) - g_{Ca} m_\infty(V)(V - E_{Ca}),$$
$$\frac{dn}{dt} = \phi(n_\infty(V) - n)/\tau_n(V), \tag{70}$$

where

$$m_\infty(V) = \frac{1}{2}\left[1 + \tanh((V - V_1)/V_2)\right]$$
$$\tau_n(V) = 1/\cosh((V - V_3)/(2V_4)) \tag{71}$$
$$n_\infty(V) = \frac{1}{2}\left[1 + \tanh((V - V_3)/V_4)\right]$$

V is the membrane potential, C is the membrane capacitance, I is the applied current, and g_L, g_{Ca}, and g_K are the peak conductances of leak, calcium, and potassium, respectively. The variable n represents the potassium recovery variable, with m_∞ and n_∞ representing the steady state equations for the calcium and potassium gating variables, respectively. The voltage variables E_L, E_{Ca}, E_K represent the respective Nernst potentials of each ion. The remaining voltage variables, V_1 through V_4, determine the phase-plane properties of the model. The variable ϕ depends heavily on temperature and affects the time constant, τ_n, for the recovery variable, n, and in effect determines how quickly the membrane potential recovers.

In phase space, ϕ controls the bifurcation regime and I serves as a bifurcation parameter within each regime. There are three main regimes of the ML system: Hopf, saddle-node on an invariant circle (SNIC), and homoclinic. The

regime is controlled by the parameter ϕ, and bifurcations within each regime

is controlled by I_{app} (Table 1).

Table 1: Parameter values for the Morris-Lecar model [8].

Parameter	Hopf	SNIC	Homoclinic
ϕ	0.04	0.067	0.23
g_{Ca}	4.4	4	4
V_3	2	12	12
V_4	30	17.4	17.4
E_{Ca}	120	120	120
E_K	-84	-84	-84
E_L	-60	-60	-60
g_K	8	8	8
g_L	2	2	2
V_1	-1.2	-1.2	-1.2
V_2	18	18	18
C_m	20	20	20

A.2.2   McKean

The McKean model, first studied by Henry McKean [13], was introduced as

a piecewise linear analog to planar conductance-based models such as the

Morris-Lecar model. We use the parameters in Table 2.

The model equations are,

$$C\dot{v} = f(v) - w + I,$$

$$\dot{w} = g(v, w),$$

(72)

where the functions f and g are given by

$$f(v) = \begin{cases} -v, & v < a/2 \\ v - a, & a/2 \leq v \leq (1+a)/2 \\ 1 - v, & v > (1+a)/2 \end{cases} , \tag{73}$$

and

$$g(v, w) = v - \gamma w. \tag{74}$$

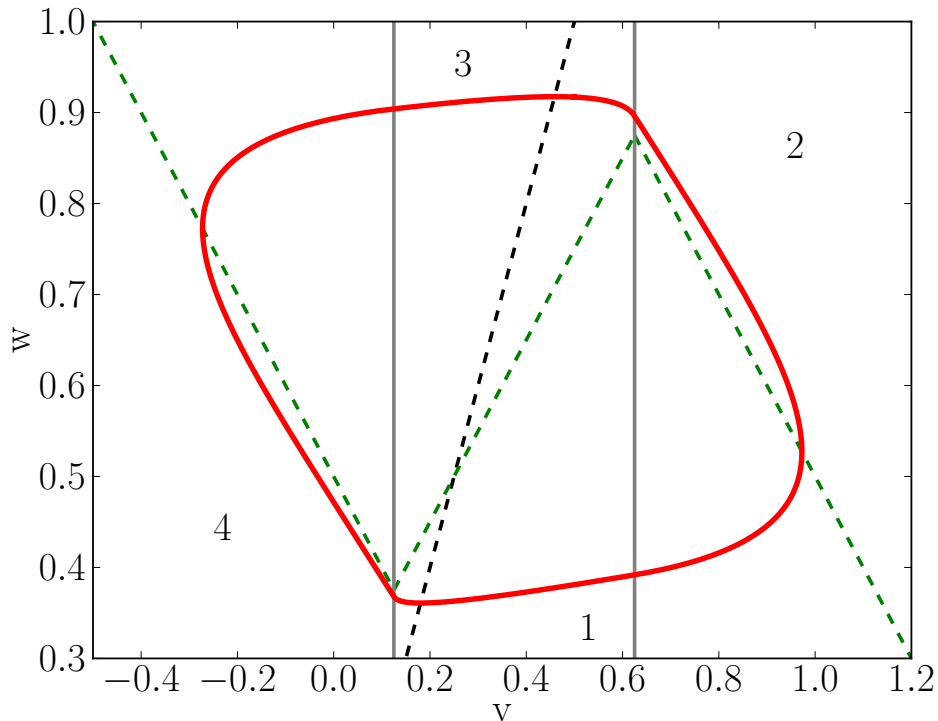Figure A.1 illustrates the (v, w) phase plane for the McKean model.

Figure A.1: McKean model. The black and green dashed lines represent the nullclines. The red loop represents the limit cycle. Vertical gray lines denote the boundaries between each region (labeled 1 through 4) [6]. Copyright © 2008 Society for Industrial and Applied Mathematics. Reprinted with permission. All rights reserved.

Table 2: Parameter values for the McKean model [6].

Parameter	Value
γ	.5
C	.1
a	0.25

A.2.3   Piecewise Linear Morris-Lecar

The Piecewise Linear Morris-Lecar system (PML system), studied in [6], is a PWL approximation to the Morris-Lecar model. We were motivated to study this model because of the relative simplicity of the equations and the availability of closed-form expressions for the iPRC and trajectories in phase space, from [6]. The iris system, a PWL approximation of the sine system, provided insight into the behavior of the iPRC of the sine system. We hoped to gain similar insight into the Morris-Lecar model by analyzing the PML model.

The equations for Coombes's PML model are the same as for the system in Eq. (72), with parameters defined in Table 1. The function $f(v)$ is defined as in the McKean model, and $g(v, w)$ is given by [6]:

$$
g(v, w) = \begin{cases} (v - \gamma_1 w + b^*\gamma_1 - b)/\gamma_1, & v < b \\ (v - \gamma_2 w + b^*\gamma_2 - b)/\gamma_2, & v \geq b \end{cases}
$$

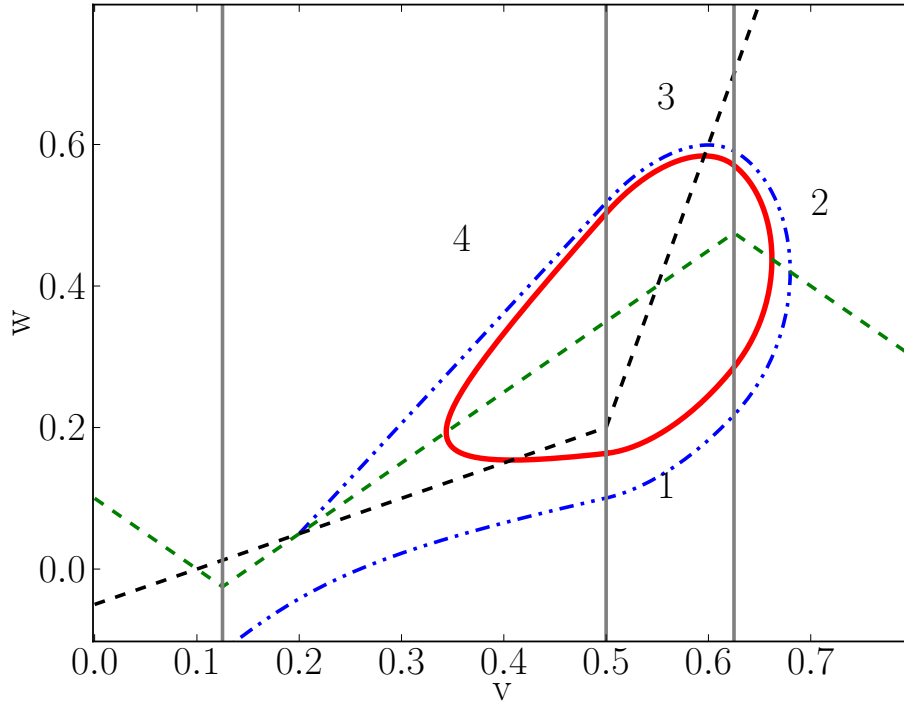The nullclines are easily computed by hand and are illustrated in A.2.

Figure A.2: Piecewise linear Morris-Lecar model. The black and green dashed lines represent the nullclines. The red loop represents the limit cycle, with the separatrix (represented by the blue dot-dot-dash), dividing the set of points that converge to the fixed point to the far left with points in the basin of attraction of the limit cycle. Vertical gray lines denote the boundaries between each region (labeled 1 through 4). The boundary between regions 4 and 1 is denoted v_{th}^1 and the boundary between regions 1 and 2 is denoted v_{th}^2 [6].

Table 3: Parameter values of the PML model (Fig. A.2) [6].

Parameter	Value
γ_1	2
γ_2	0.25
C	0.825
a	0.25
b	0.5
b^*	0.2

A.2.4 Sine System

In [20], Shaw et al. constructed the "sine system" as a nominal model for systems with one-parameter families of limit cycles approaching close to a sequence of fixed points [20]. The sine system is a smooth planar system of autonomous ordinary differential equations defined as

$$
\begin{aligned}
\frac{dy_1}{dt} &= f(y_1, y_2) = \cos(y_1)\sin(y_2) + \alpha\sin(2y_1), \\
\frac{dy_2}{dt} &= g(y_1, y_2) = -\sin(y_1)\cos(y_2) + \alpha\sin(2y_2).
\end{aligned}
\tag{75}
$$

As written, the system forms a stable heteroclinic cycle, a special case of a heteroclinic channel [1], where one unstable manifold of one saddle becomes the stable manifold of a neighboring saddle. Limit cycles are introduced by breaking the heteroclinic cycle by perturbing the vector field by introducing an orthogonal component, whose magnitude is controlled by the parameter μ. These limit cycles have a close passage to each of the four saddle points in the system [19].

$$
\begin{aligned}
\frac{dy_1}{dt} &= f(y_1, y_2) + \mu g(y_1, y_2), \\
\frac{dy_2}{dt} &= g(y_1, y_2) - \mu f(y_1, y_2),
\end{aligned}
\tag{76}
$$

where $1 > \mu > 0$. For any small $\mu > 0$, there exists a stable limit cycle with diverging period as $\mu \to 0$.

A.2.5   Iris System

In order to derive analytical results, one may approximate the sine system
with the iris system, a PWLDS [20]. We use a linearization about one of
the saddles in the sine system to construct four consecutive PWL regions,
each a 90-degree rotation of the previous square. For the sake of simplicity, we
focus our analysis to the southwesterly (SW) iris square, and inject trajectories
exiting the iris square (along the top edge) directly into the right edge of the
same iris square, with a fixed offset $a \geq 0$. Let $\lambda > 1$. The nondimensionalized
form of the iris equation is

$$\begin{aligned}
\frac{ds}{dt} &= -\lambda s, \\
\frac{du}{dt} &= u.
\end{aligned} \tag{77}$$

Given initial condition $u(0) = u_0$ (and $s(0) \equiv 1$), if the first egress time
is $T_1 = \ln(1/u_0)$, with egress location $s(T_1^-) = u_0^\lambda$ (and $u(T_1^-) \equiv 1$), then
after applying the offset the trajectory is reinjected at position $u_1 = u(T_1^+) =$
$s(T_1^-) + a = u_0^\lambda + a$. Applying this procedure inductively, the successive
injections occur at locations $u_{k+1} = u_k^\lambda + a$ and times $T_{k+1} = T_k + \ln(1/u_k)$.
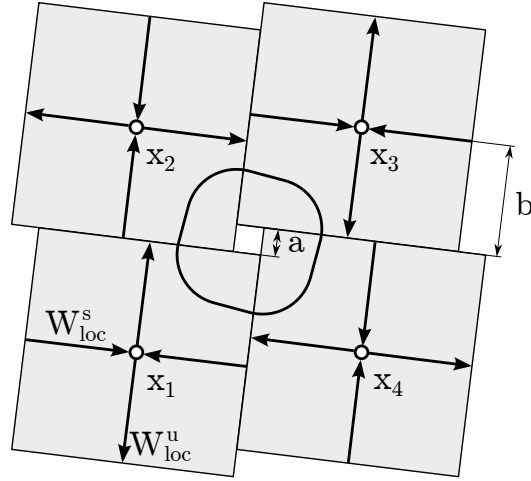
Figure A.3: Construction of the iris system. The SW square is defined by the system in Eq. (77). The remaining squares are defined by consecutive 90-degree clockwise rotation with a translation of system (77). The parameter a acts as the bifurcation parameter (when $a = 0$, there is a heteroclinic cycle), and the parameter $b = 1$. The unstable and stable manifolds of the saddle x_1 is denoted W_{loc}^u and W_{loc}^s, respectively. The loop passing through each region is an example of how a limit cycle might appear [20]. Copyright © 2012 Society for Industrial and Applied Mathematics. Reprinted with permission. All rights reserved.

A.3   Analytic, Piecewise Continuous Infinitesimal Phase Response Curve of the Iris System

A.3.1   Summary of Shaw et al 2012

In [20], Shaw et al derived several analytical results for the iPRC of the iris system (see Appendix A.2.5 for the definition). The central result is a theorem which we summarize in three points. Let $\lambda > 1 > a > 0$.

1. If the function $\rho(u) = u^\lambda - u + a$ has two isolated positive roots, then the iris system has a stable limit cycle Moreover, the limit cycle trajectory

enters each square at local coordinates $(1, u)$, where u is one of the roots, and exits the square at local coordinates $(s, 1)$, where $s = u^\lambda$. The period of the limit cycle is $T = 4\log(1/u)$.

2. The iPRC of the iris system, for perturbations in direction $\eta = (\eta_s, \eta_u)$ is

$$Z(\eta, \phi, a) = \frac{\eta \cdot \beta(\phi)}{\log(1/u)(u - \lambda s)}, \tag{78}$$

where $\phi = t/T$ is the phase, $\beta(\phi) = (s^{(1-\phi)}, u^\phi)$ and η is a unit vector in the L_1 norm.

3. The infinitesimal phase response to perturbations parallel to the unstable eigendirection in a given square diverges in the limit as $a \to 0$, and the response to perturbations parallel to the stable eigendirection diverges when $\phi \in (1 - 1/\lambda, 1)$; otherwise, the iPRC converges to zero as $a \to 0$.

See Fig. A.4 for a geometric interpretation of this theorem.

In order to gain a broader understanding of potential biological applications of these results and whether these results hold in general, we applied the same numerical tools to the Morris-Lecar system. The Morris-Lecar system (defined in Appendix A.2.1) is a neurobiologically relevant dynamical system based on barnacle muscle. The model is capable of several bifurcations, which include a hopf, saddle-node on a limit cycle (SNLC), and homoclinic bifurcation. We focus on the homoclinic bifurcation because it provides an example of a family
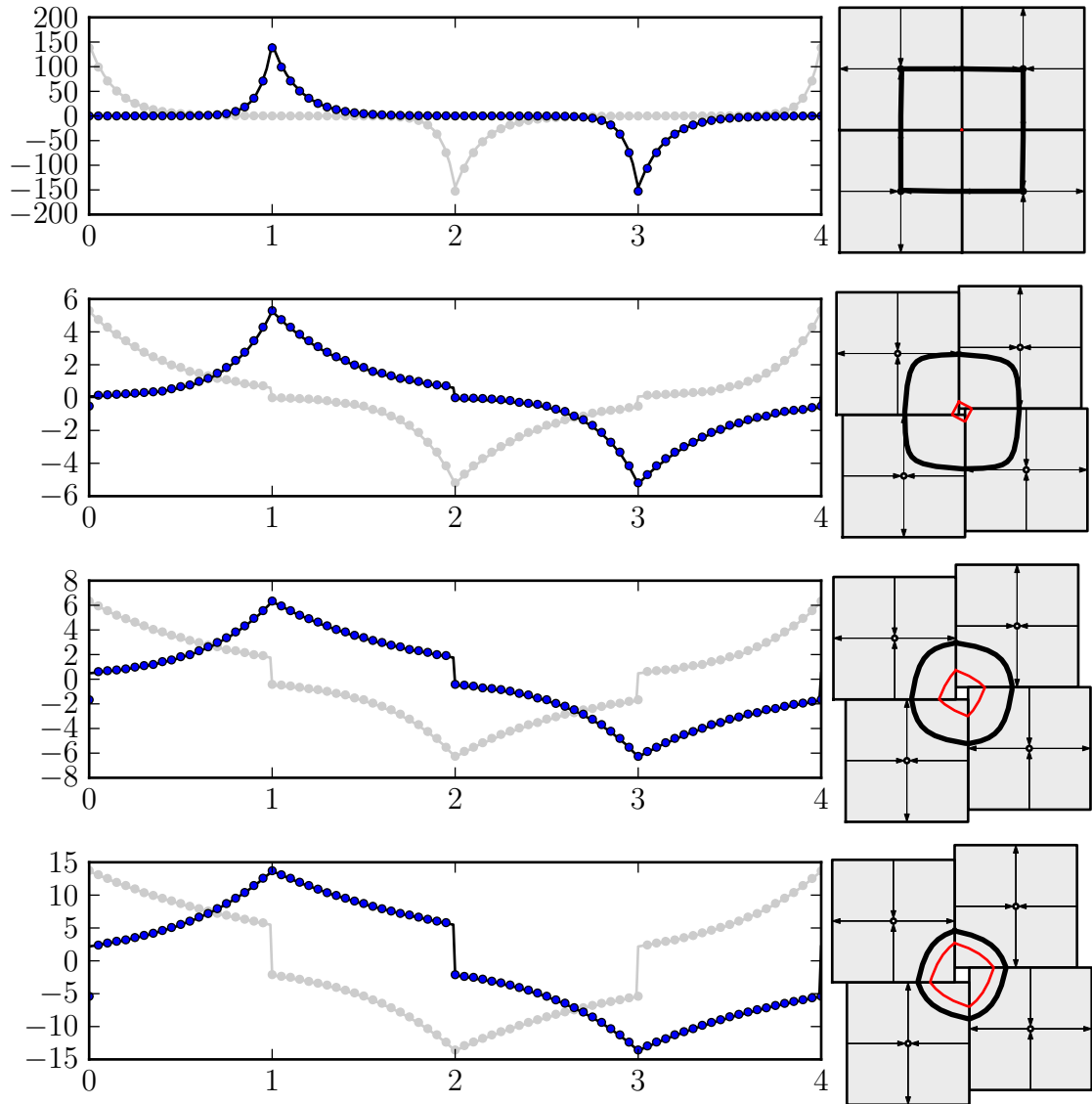
Figure A.4: Divergence of the iris iPRC in the heteroclinic limit. As the theorem predicts, we have divergence of the iPRC of the iris system in the approach to the heteroclinic bifurcation. The left column shows plots of the iPRC with phase change on the vertical axis and phase on the horizontal axis. Dots represent values from numerical simulations and lines represent the analytic solution. Bifurcation parameter values from top to bottom: $a = 10^{-3}, 0.1, 0.2,$ and 0.24 [20]. Copyright © 2012 Society for Industrial and Applied Mathematics. Reprinted with permission. All rights reserved.

of limit cycles passing close to a single fixed point. Once we are in a particular

bifurcation regime, we generate limit cycles by varying a bifurcation parameter,

I_{app}, which represents the current applied to the cell.

We used the python packages numpy and scipy to run perturbation analyses on the limit cycle of the Morris-Lecar model in the homoclinic regime. Given a bifurcation parameter value I_{app} (chosen such that a stable limit cycle exists) and a particular phase along the limit cycle, we use a perturbation of size 1×10^{-4} to estimate the change in timing at that phase. By taking this analysis close to the homoclinic bifurcation, we find that the behavior of the iPRC in the approach to the homoclinic bifurcation closely resembles that of the analytic results of the iris system. The peak sensitivity appears to diverge in the limit of the homoclinic bifurcation, while regions of relatively small sensitivity widen and dominate the behavior in the same homoclinic limit.

Since the Morris-Lecar equation is nonlinear, it is virtually impossible to derive analytical results for the iPRC near the homoclinic bifurcation. However, the ever-lengthening regions of relatively small phase change suggest a different approach to understanding what happens to the shape of the iPRC in the limit of the homoclinic bifurcation. The long, flat regions of the iPRC are a result of trajectories spending long times in a small neighborhood in phase space, so it is likely that trajectories spend long times in the neighborhood of the saddle. If we can view the iPRC in terms of a variable that takes space into account instead of time, we may be able to more precisely calculate the shape of the iPRC in the limit of the homoclinic bifurcation. Therefore, in future work, we hope to gain greater understanding of the limit behavior of
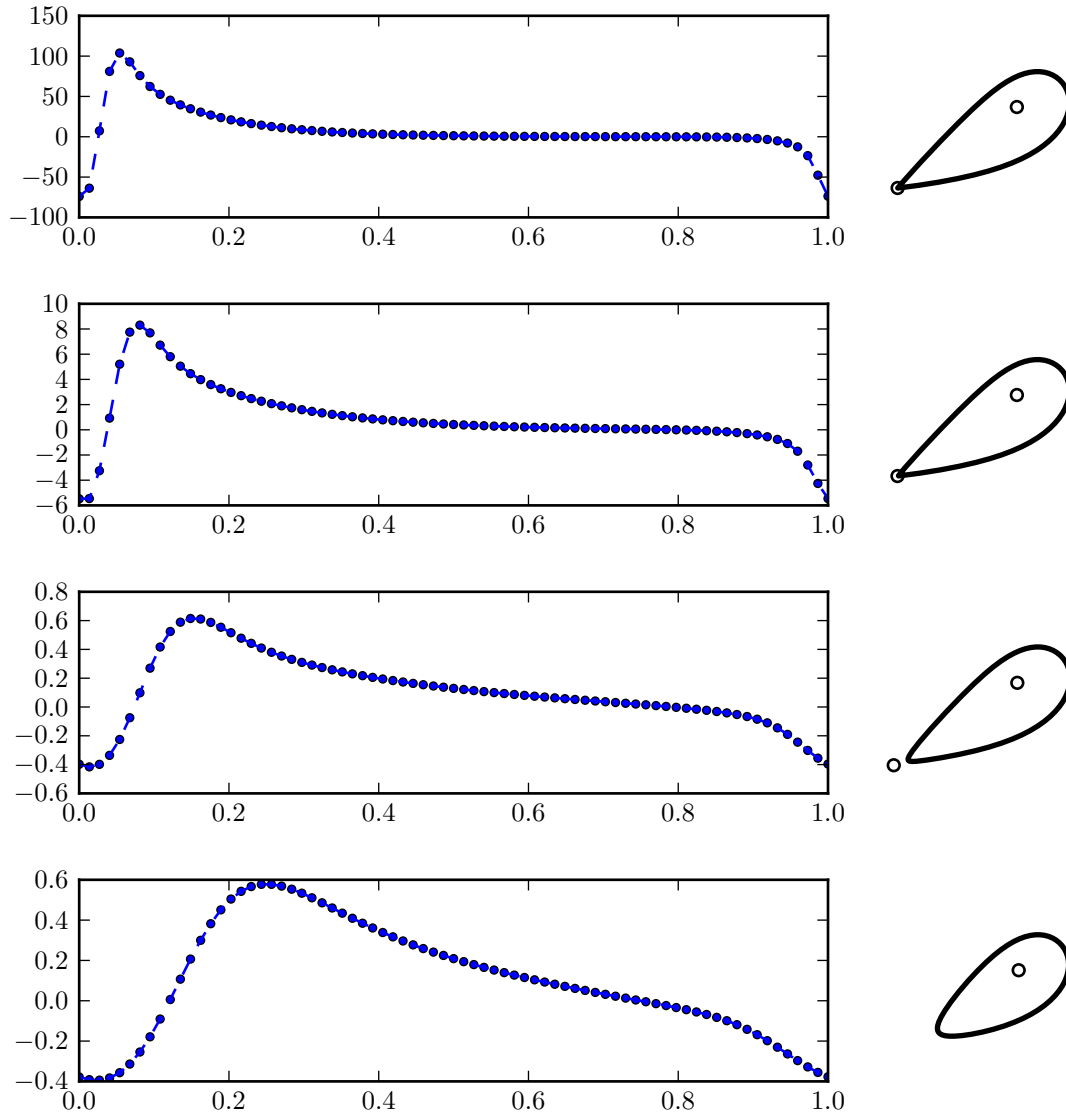
Figure A.5: Divergence of the Morris-Lecar iPRC in the homoclinic limit. The left column shows plots of the iPRC with phase change on the vertical axis and phase on the horizontal axis. Zero phase, $\phi = 0$, defined to be peak voltage. Perturbations of size 10^{-4} were used to construct the iPRC. Bifurcation parameter values from bottom to top: $I_{app} = 40, 36.2, 35.05$, and 35.009. The bifurcation is near $I_{app} = 35.0067$. The right column shows the corresponding limit cycle in phase space [20]. Copyright © 2012 Society for Industrial and Applied Mathematics. Reprinted with permission. All rights reserved.

the iPRC in this case, by analysis of the phase response curve as a function of

arc length rather than of phase.

A.4 Normal Forms and Explicit Expressions for the Infinitesimal Phase Response Curve

There are only a few cases where we can solve for the iPRC explicitly for smooth systems [8]. Here we provide examples of explicit iPRCs which arise from normal forms for systems close to a particular bifurcation.

A.4.1 Class I Excitability

Systems that always exhibit phase advance for perturbations along all phases are known as class I excitable systems. Such systems typically make the transition from excitability to steady oscillation by way of a saddle-node-on-invariant circle (SNIC) bifurcation [2]. The solution to the adjoint equation for the normal form a system at such a bifurcation is proportional to [7]

$$z(\theta) \propto 1 - \cos(\theta). \tag{79}$$

A.4.2 Supercritical Hopf Bifurcation

A model exhibits a supercritical Hopf bifurcation when the variation of a bifurcation parameter moves eigenvalues of a stable fixed point across the imaginary axis, leading to stable oscillations and an unstable fixed point. The iPRC for models close to supercritical Hopf bifurcations may be approximated

by a pure sinusoid [2, 14].

$$z(\theta) \propto \sin(\theta). \tag{80}$$

References

[1] Valentin Afraimovich, Irma Tristan, Ramon Huerta, and Mikhail I Rabi-novich. Winnerless competition principle and prediction of the transient dynamics in a lotka-volterra model. *Chaos*, 18(4):043103, Dec 2008.

[2] Eric Brown, Jeff Moehlis, and Philip Holmes. On the phase reduction and response dynamics of neural oscillator populations. *Neural Comput*, 16(4):673–715, Apr 2004.

[3] Robert J. Butera Jr., John Rinzel, and Jeffrey C. Smith. Models of Respiratory Rhythm Generation in the preBötzinger Complex. I. Bursting Pacemaker Neurons. *J Neurophysiol*, 82(1):382–397, 1999.

[4] Robert J. Butera Jr., John Rinzel, and Jeffrey C. Smith. Models of Respiratory Rhythm Generation in the preBötzinger Complex. II. Populations of Coupled Pacemaker Neurons. *J Neurophysiol*, 82(1):398–415, 1999.

[5] A H Cohen, G B Ermentrout, T Kiemel, N Kopell, K A Sigvardt, and T L Williams. Modelling of intersegmental coordination in the lamprey central pattern generator for locomotion. *Trends Neurosci*, 15(11):434–8, Nov 1992.

[6] S. Coombes. Neuronal networks with gap junctions: A study of piecewise linear planar neuron models. *SIAM Journal on Applied Dynamical Systems*, 7:1101–1129, 2008.

[7] B Ermentrout. Type I membranes, phase resetting curves, and synchrony. *Neural Comput*, 8(5):979–1001, Jul 1996.

[8] G. Bard Ermentrout and David H. Terman. *Foundations Of Mathematical Neuroscience*. Springer, 2010.

[9] Aleksei Fedorovich Filippov. *Differential Equations with Discontinuous Righthand Sides*. Mathematics and Its Applications. Kluwer Academic Publishers, Dordrecht, The Netherlands, 1988.

[10] J. Gebert, N. Radde, and G.-W. Weber. Modeling gene regulatory networks with piecewise linear differential equations. *European Journal of Operational Research*, 181(3):1148 – 1165, 2007.

[11] Leon Glass and Stuart A. Kauffman. The logical analysis of continuous, non-linear biochemical control networks. *Journal of Theoretical Biology*, 39(1):103 – 129, 1973.

[12] J. Guckenheimer. Isochrons and phaseless sets. *Journal of Mathematical Biology*, 1:259–273, 1975. 10.1007/BF01273747.

[13] McKean H.P. Nagumo's equation. *Advances in Mathematics*, 4:209–223, 1970.

[14] Eugene M. Izhikevich. *Dynamical Systems in Neuroscience: The Geometry of Excitability and Bursting*. Computational Neuroscience. MIT Press, Cambridge, Massachusetts, 2007.

[15] James P. Lund and Arlette Kolta. Generation of the central masticatory pattern and its modification by sensory feedback. *Dysphagia*, 21(3):167–174, 2006.

[16] C. Morris and H. Lecar. Voltage oscillations in the barnacle giant muscle fiber. *Biophysical Journal*, 35(1):193 – 213, 1981.

[17] B.E. Paden and S.S. Sastry. A calculus for computing Filippov's differential inclusion with application to the variable structure control of robot manipulators. *Circuits and Systems, IEEE Transactions on*, 34(1):73–82, 1987.

[18] Octavia Plesh, Beverly Bishop, and Willard McCall. Effect of gum hardness on chewing pattern. *Experimental Neurology*, 92(3):502 – 512, 1986.

[19] J. Reyn. Generation of limit cycles from separatrix polygons in the phase plane. In Rodolfo Martini, editor, *Geometrical Approaches to Differential Equations*, volume 810 of *Lecture Notes in Mathematics*, pages 264–289. Springer Berlin / Heidelberg, 1980. 10.1007/BFb0089983.

[20] Kendrick M. Shaw, Young-Min Park, Hillel J. Chiel, and Peter J. Thomas. Phase resetting in an asymptotically phaseless system: On the phase response of limit cycles verging on a heteroclinic orbit. *SIAM Journal on Applied Dynamical Systems*, 11(1):350–391, March 13 2012.

[21] Lucy E. Spardy, Sergey N. Markin, Natalia A. Shevtsova, Boris I. Prilutsky, Ilya A. Rybak, and Jonathan E. Rubin. A dynamical systems analysis

of afferent control in a neuromechanical model of locomotion. I. Rhythm generation. *Journal of Neural Engineering*, 8(6):065003, Dec 2011.

[22] Lucy E. Spardy, Sergey N. Markin, Natalia A. Shevtsova, Boris I. Prilutsky, Ilya A. Rybak, and Jonathan E. Rubin. A dynamical systems analysis of afferent control in a neuromechanical model of locomotion. II. Phase asymmetry. *Journal of Neural Engineering*, 8(6):065004, Dec 2011.